British Journal of Cancer

ARTICLE

Cellular and Molecular Biology

Capecitabine induces hand-foot syndrome through elevated thymidine phosphorylase-mediated locoregional toxicity and GSDME-driven pyroptosis that can be relieved by tipiracil

Bingxue Yang[1], Xinran Xie[2], Dazhao Lv[2], Jiajun Hu[2], Yuyun Chen[2], Zhaoyu Wu[2], Shuyue Luo[2] and Shiyi Zhang[2]✉

A : Hand-foot syndrome (HFS) is a serious dose-limiting cutaneous toxicity of capecitabine-containing chemotherapy, leading to a deteriorated quality of life and negative impacts on chemotherapy treatment. The symptoms of HFS have been widely reported, but the precise molecular and cellular mechanisms remain unknown. The metabolic enzyme of capecitabine, thymidine phosphorylase (TP) may be related to HFS. Here, we investigated whether TP contributes to the HFS and the molecular basis of cellular toxicity of capecitabine.

: *TP-/-* mice were generated to assess the relevance of TP and HFS. Cellular toxicity and signalling mechanisms were assessed by in vitro and in vivo experiments.

: *TP-/-* significantly reduced capecitabine-induced HFS, indicating that the activity of TP plays a critical role in the development of HFS. Further investigations into the cellular mechanisms revealed that the cytotoxicity of the active metabolite of capecitabine, 5-DFUR, was attributed to the cleavage of GSDME-mediated pyroptosis. Finally, we demonstrated that capecitabine-induced HFS could be reversed by local application of the TP inhibitor tipiracil.

: Our findings reveal that the presence of elevated TP expression in the palm and sole aggravates local cell cytotoxicity, further explaining the molecular basis underlying 5-DFUR-induced cellular toxicity and providing a promising approach to the therapeutic management of HFS.

British Journal of Cancer (2023) 128:219–231; https://doi.org/10.1038/s41416-022-02039-3

Capecitabine is a widely used oral prodrug of 5-fluorouracil (5-FU) that is effective in the treatment of a number of cancers [1–3]. With more patients benefiting from treatment, treatment-related toxicity and quality of life have become increasingly relevant [4]. Hand-foot syndrome (HFS), also called palmar-plantar erythrodysesthesia, is a distinctive and frequently occurring dermatologic toxic reaction associated with capecitabine [5–7]. The rate of HFS induced by capecitabine ranges from 50% to 71%, and the rate of severe HFS (>grade 3) ranges from 10% to 17% [5, 8, 9].

Initial symptoms of HFS are dysesthesia, tingling in the palms, fingers, and soles of the feet, and erythema, which may progress to extremely painful and debilitating conditions if not given prompt management [10, 11]. The histology of HFS shows a nonspecific pattern of inflammatory disorders, such as necrotic and dyskeratotic keratinocytes, dermal oedema, blood vessel dilation and perivascular lymphocytic infiltrate [12–14]. Although HFS is not life-threatening, it can be very painful and cause significant discomfort, which may seriously impact the quality of life [10, 15].

For patients experiencing HFS, the only effective treatment option is dose modification, including dose reduction or treatment interruption, which may have negative impacts on the efficacy of the patient's antitumor therapy [16, 17]. Therefore, studying the pathogenesis of HFS and providing treatment approaches based on its mechanistic occurrence are urgently needed to improve the quality of life and treatment tolerance.

Capecitabine is a prodrug of 5-FU. Capecitabine is designed to preferentially generate 5-FU in tumour tissue *via* a three-step enzymatic process (Fig. 1a) [1, 18]. Capecitabine is first hydrolysed by carboxylesterase in the liver to the intermediate 5′-deoxyfluorocytidine (5-DFCR), and then it undergoes deamination by cytidine deaminase, which is highly active in the liver and tumour tissue. The resulting molecule, 5′-deoxyfluorouridine (5-DFUR), is further converted to 5-FU by thymidine phosphorylase (TP), which is present at significantly high concentrations in tumour tissue, and then the locally generated 5-FU kills the surrounding cancer cells [18]. Subsequently, 5-FU is metabolised by dihydropyrimidine dehydrogenase (DPD) to inactive metabolites, most of which are excreted in urine [19].

[1]School of Pharmacy, Shanghai Jiao Tong University, Shanghai, China. [2]School of Pharmacy and School of Biomedical Engineering, Shanghai Jiao Tong University, 200240 Shanghai, China. ✉email: zhangshiyi@sjtu.edu.cn

Received: 15 April 2022 Revised: 17 September 2022 Accepted: 19 October 2022
Published online: 8 November 2022

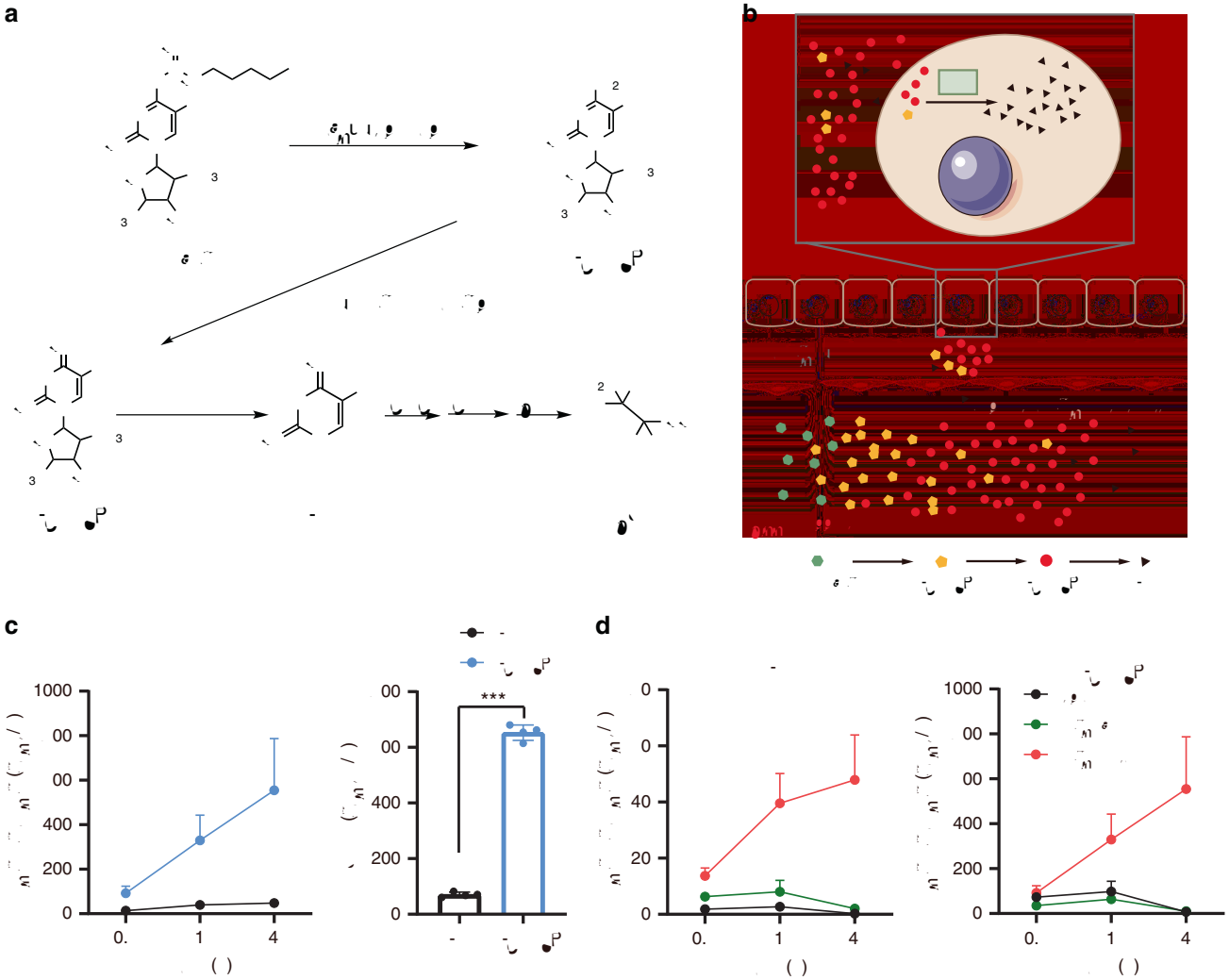

Fig. 1 Metabolic pathway of capecitabine. 5-DFCR 5′-deoxy-5-fluorocytidine, 5-DFUR 5′-deoxy-5-fluorouridine, DPD dihydropyrimidine dehydrogenase, TP thymidine phosphorylase, FBAL α-fluoro-β-alanine. Schematic representation of the relative concentration of capecitabine and its metabolites in blood and skin tissue. Mean profiles of 5-DFUR and 5-FU in skin of palm after oral administration of capecitabine 1000 mg/kg to BALB/c mice for 5 days ($n = 4$). Concentrations of 5-DFUR and 5-FU in plasma, skin of back and skin of palm after oral administration of capecitabine 1000 mg/kg to BALB/c mice for 5 days. *$P < 0.05$; **$P < 0.01$; ***$P < 0.001$; ns, no significant difference.

The mechanism for capecitabine-induced HFS appears to be associated with the activity of the enzymes responsible for the metabolism of capecitabine. Clinical pharmacokinetics studies of capecitabine showed that 5-DFCR and 5-DFUR are the dominant forms of metabolites rather than 5-FU in plasma (Fig. S1A) [20]. The concentration of 5-FU in plasma was considerably lower than that of its direct precursor 5-DFUR [20], suggesting that more 5-DFUR, rather than 5-FU, enters and accumulates in the skin (Fig. 1b) or other normal tissues. The systemic exposure concentrations of 5-DFUR and 5-FU may at least partially support the hypothesis that treatment-related HFS is dependent on the activity of TP.

Moreover, two recent clinical studies have investigated the role of TP levels in HFS. Patients with HFS had higher TP and lower DPD levels in tumours than those without HFS, but the differences were not significant [21]. Considering that keratinocytes express various metabolic enzymes [22–24], its metabolism within the skin may be an essential step in the manifestation of the cutaneous toxicity of capecitabine. Increased levels of 5-FU as a result of local elevated TP activity may be important in capecitabine-induced HFS. Consistent with this idea, a study conducted on healthy volunteers ($n = 12$) revealed that TP was more highly concentrated in the palmar skin than the back skin [25]. Accordingly, 5-FU accumulation in the target skin can be an important factor in capecitabine-induced cutaneous adverse reactions. These findings demonstrate the potential correlation between the activity of TP and HFS. However, direct evidence that the activity of TP is critical in the onset of HFS is lacking. It is necessary to determine whether the expression of TP plays a role and to fully clarify the cause and pathogenesis of capecitabine-related HFS.

The differences in the local concentration of 5-FU could not fully explain the manifestations of inflammation in HFS. The mechanism of inflammation resulting from capecitabine and its metabolites is not well clarified. It has long been believed that apoptosis is responsible for chemotherapy-induced cytotoxicity [26]. However, apoptosis does not induce any inflammatory reaction. Pyroptotic cell death as a novel killing mechanism of chemotherapy has been previously reported [27–29]. Recent research suggests that chemotherapy could induce pyroptosis in normal cells with high expression of GSDME, which may be one of the causes of the inflammatory reactions associated with chemotherapy [30]. Compared with *GSDME* + / + mice, *GSDME*-/-

mice exhibited less intestinal and lung injury after treatment with chemotherapy agents [30]. In addition, fluorouracil could induce pyroptosis rather than apoptosis in gastric cancer cells, which promoted the induction of sustainable antitumor immunity [31]. HFS is a type of dermatitis accompanied by local inflammation and pain, but how the toxicity of capecitabine and its metabolites translates into persistent inflammation and develops into HFS has not been reported or studied. Increasing evidence has shown that pyroptosis plays a critical role in the pathogenesis of inflammatory diseases [32]. Excessive pyroptosis is often associated with robust inflammation that can result in a number of inflammatory diseases, such as chronic colitis [33], acute liver failure [34] and atherosclerosis [35]. These studies show the important effects of pyroptosis in chemotherapy and inflammatory diseases, which offer new insight into the mechanism of chemotherapy-induced toxicity. Thus, we hypothesised that pyroptosis might be involved in the development of capecitabine-induced HFS.

In this study, we detected the relative content of 5-DFUR and

AACCTTCCAAAGATG-3′, reverse, 5′-GCTTGTTCCTCACTACTCTCAAAT-3′; human IL-18: forward, 5′-GACCAAGTTCTCTTCATTGACCAAG-3′, reverse, 5′-GATAGTT ACAGCCATACCTCTAGGC-3′; human GrB: forward, 5′-TTCGTGCTGACAGCTGCT CACT-3′, reverse, 5′-CTCTCCAGCTGCAGTAGCATGA-3′.

. x fl x

Cells were fixed with 4% (w/v) paraformaldehyde (10 min at room temperature), washed twice with PBS, and permeabilized using 0.2% Triton X-100 (15 min at room temperature). Coverslips were washed with PBS, saturated with 3% BSA/PBS for 1 h at room temperature, and incubated with anti-GrB antibody overnight at 4 °C. After washing four times with PBST, cells were incubated with Alexa-conjugated secondary antibody (Thermo Fisher Scientific, A11034) for 1 h at room temperature. After washing, the coverslips were sealed and examined with a digital pathology scanning 138 system (NANOZOOMER S360, Leica).

. x W - x . x x, W

The supernatants of HaCaT cells were collected to determine the level of IL-1β, IL-6 and IL-18. The protein levels of IL-1β, IL-6 and IL-18 were measured using enzyme-linked immunosorbent assay (ELISA) kits (Shanghai Enzyme-linked Biotechnology, China) according to the manufacturer's instructions. The plates were read at 450 nm using a multifunction microplate reader (Infinite M200 Pro, Tecan).

A

Female BALB/c mice and female BALB/C nude mice free of murine viruses, bacteria and parasites and 6–8 weeks of age on arrival, were purchased from Shanghai Jihui Laboratory Animal Care (China). The mice were maintained in cages on a 12-h light/dark schedule for one week. Animals were cared for in accordance with the institutional guidelines of East China Normal University for the care and use of experimental animals.

. x

Six-week-old female BALB/c mice were used to establish the HFS model. Mice were administered with capecitabine at 1000 mg/kg p.o. once daily. The paw skin changes like scaling were visually inspected by at least two researchers every day and photographed when grade changes were observed. HFS grade evaluation: Grade 0-normal; Grade 1-slight desquamation or dry lines; Grade 2-desquamation, erythema or swelling; Grade 3-severe peeling and erythema.

Generation of TP-/- *mice and treatment*. *TP-/-* mice were generated by co-microinjection of in vitro translated Cas9 mRNA and gRNAs into BALB/C zygotes, as described for *TP-/-* mice [36]. The targeting strategy, including the gRNA sequences and the knockout allele obtained, are depicted in supplementary information Fig. S3. Germ line transmission of the mutation was verified by PCR analysis of tail DNA. The presence of the wild-type allele and the disrupted allele was determined by allele-specific PCR analysis. The primer upstream of the disruption site, TCGGGACCCATAGA-TACCAAGACCC (oligonucleotide TP-WT-F), and the primer downstream of the disruption site, CACCTTCATTAACTTCTAGGGACGG (oligonucleotide TP-Mut-R), were used to identify homozygous species.

TP-/- and wild-type mice were administered with capecitabine at 1000 mg/kg p.o. once daily. The control wild-type mice were administered with solvent p.o. once daily. The HFS grade of paw skin was visually inspected by at least two researchers every day and photographed. At the end of experiment, euthanasia was performed using CO_2 asphyxia followed by cervical dislocation. Skin tissues of paws were then enucleated for further experiments.

Prophylactic treatment study. Six-week-old wild-type BALB/c mice were randomised into three groups. (1) CTL group: mice received Citrate buffer pH 6 plus 5% gum Arabic solution v/v without capecitabine. (2) CAP-Vehicle group: mice received capecitabine and topical gel without active ingredients. (3) CAP-TPI group: mice received capecitabine and topical gel with 2% tipiracil. After intragastric administration, the paws of the mice were coated with the corresponding gel and wrapped with gauze. After gel application, mice were fitted with Elizabethan collars (Kent Scientific) to reduce the likelihood of oral ingestion. The HFS grade of paw skin was visually inspected by at least two researchers every day and photographed. At the end of experiment, euthanasia was performed using CO_2 asphyxia followed by cervical dislocation. Skin tissues of paws were then enucleated for further experiments.

The xenograft tumour model and treatment. Six-week-old female BALB/C nude mice were used as a tumour xenograft model to test the influence of TPI gel on the antitumor effect of capecitabine.

Mice were injected subcutaneously in the right axilla with 1×10^6 HCT 116 cells in a volume of 100 µL PBS. Tumour volumes were measured in two dimensions with calipers and calculated with the formula $(L \times W^2)/2$, where L is length and W is width of the tumour, respectively. Mice were randomised into three groups after tumour had been established in two weeks after tumour cell inoculation: (1) CTL group: mice received Citrate buffer pH 6 plus 5% gum Arabic solution v/v without capecitabine. (2) CAP-Vehicle group: mice received capecitabine and topical vehicle gel without active ingredients. (3) CAP-TPI group: mice received capecitabine and topical gel with 2% tipiracil. Capecitabine was administered orally once daily for 21 days at dose levels of 180 mg/kg body weight starting in 200 µL above mentioned 1× solution. TPI or vehicle gel was topically applied on the paws of mice for 4 h once a day for 21 days. The body weight and tumour volume were recorded every 2 days. Mice were sacrificed and dissected to measure the tumour weight.

W

The paws were harvested from mice under different treatments. The mice paw samples were fixed in 4% paraformaldehyde and embedded in paraffin for hematoxylin and eosin (H&E) and immunostaining. For H&E staining, paraffin sections were cut at 4 µm and stained using standard methods. For immunohistochemical staining, 4 µm of paraffin sections were air-dried and then incubated with Ki67 (1:100), CD3 (1:100), F4/80 (1:100) antibodies (Servicebio, China) for overnight at 4 °C. The stained slides were rinsed with PBST and incubated with HRP labelled goat anti-rabbit or mouse IgG (1:200; Zsbio, China) for 30 min at room temperature. After a rinse with PBST, the slides were incubated with DAB (Zsbio, China) for visualisation. Subsequently, the slides were counterstained with Harris' Hematoxylin for 10 s and washed with tap water. EdU incorporation is detected by Click-It EdU Alexa Fluor 594 Imaging Kit (Invitrogen). 5-Ethynyl-2′-deoxyuridine (EdU) was administered via i.p. injection (50 mg/kg). Sections were visualised under a digital pathology scanning 138 system (NANOZOOMER S360, Leica) or Upright-Reverse Fluorecent Microscopy 139 (Revolve, Echo).

, , ,

Before each assay, animals were acclimated to the experimental conditions for 3 days (once per day). Mice were tested in a random and blinded fashion. To assay for heat pain response, heat was applied to the pad of the hind paw and withdrawal latency was measured. Mice were put onto the hot-plate set at 52 °C, and the latency to lick, flinch, or jump was measured once for each animal. Measurements at different temperatures were taken at 30 min intervals. The cut-off time was set at 20 s to avoid injury.

. x 5- x 5-

BALB/c mice were daily given oral dose of capecitabine at 1000 mg/kg for 5 days. Blood, skin of back and skin of palm were collected at intervals 0.5, 1 and 4 h after 5th dosing, four animals per time point. Blood was collected in lithium heparin, and plasma was isolated and stored at −80 °C. Skin samples were removed and snap-frozen in liquid nitrogen.

5-DFUR and 5-FU were determined in plasma and tissues using a modified version of the protocol previous published [37]. Briefly, tissue samples were homogenised using a Precellys 24 homogeniser with small-ball bearings for 2 × 50 s at 6000 rpm in ice-cold 50:50 acetonitrile water (v/v) containing 25 µg/mL tetrahydrouridine to make a final concentration of 50 mg tissue per mL. In all, 50 µL of homogenate was transferred to a clean tube prespiked with 200 µL of ice-cold acetonitrile containing 50 ng/mL stable labelled (SIL) internal standards of all 4 analytes (Toronto Research Chemicals). After centrifugation at 20,000 × g for 5 min the supernatant was evaporated to dryness, resuspended in 100 µL of water and injected onto the LC-MS/MS. For plasma samples, 50 µL of plasma was precipitated with 150 µL of acetonitrile containing 50 ng/mL stable labelled internal standards and processed similarly.

Detection was achieved by LC-MS/MS using a Thermo TSQ Vantage mass spectrometer with a HESI-II probe operated in positive and negative mode at a spray voltage of 3 kV and vaporiser temperature of 325 °C. Detection of the ions was performed in the multiple reaction monitoring mode, specific for each compound. Concentrations of 5-DFUR and 5-FU in samples were determined by comparison against calibration lines constructed using authentic reference standards.

All data were expressed as the mean value ± standard error of mean (SEM) or mean value ± standard deviation (SD). Statistical significance (*P*) was determined with unpaired *t*-test with Welch's correction, analysis of variance (ANOVA) with Dunn's multiple comparison test, ANOVA with Bonferroni correction, ANOVA with Tukey's multiple comparison test, or Gehan–Breslow–Wilcoxon test. Differences were considered significant when *P* was less than 0.05 as indicated in each figure legend.

It has been hypothesized that HFS may be associated with TP activity. Clinical pharmacokinetics studies of capecitabine showed that 5-DFUR is the dominant form of metabolites rather than 5-FU in plasma (Fig. S1A) [20]. To prove that 5-DFUR rather than 5-FU mainly reside in the skin, we measured the concentration of 5-DFUR and 5-FU in skin by using LC-MS/MS after the oral administration of capecitabine 1000 mg/kg to BALB/c mice for 5 days. As shown in Fig. 1c, the concentration and AUC of 5-FU in skin of palm was considerably lower than that of its direct precursor 5-DFUR, suggesting that more 5-DFUR, rather than 5-FU, enters and accumulates in the skin. What's more, the pharmacokinetics study of capecitabine showed the concentration of 5-DFUR and 5-FU in the paw were significantly higher than in the back skin and plasma of mice (Fig. 1d), indicating high concentration of metabolites of capecitabine aggravates local cytotoxicity. The concentrations of 5-DFUR and 5-FU in skin support that treatment-related HFS is dependent on the activity of TP.

A previous study suggested a link between the expression of TP in the palm and HFS [25], however, they did not directly investigate the involvement of TP in capecitabine-induced HFS. Therefore, more studies are needed to confirm the role of TP in the development of HFS. To investigate the effect of TP on HFS, we first compared the relative expression of TP between the palm area and dorsal area of the paw in mice. Through immunohistochemical (IHC) analysis, TP expression was found to be significantly higher in the palmar and plantar areas than in the dorsal area of the paw (Fig. 2a).

To further determine whether TP contributes to the HFS induced by capecitabine, we generated *TP-/-* mice (Fig. S3) [36]. *TP-/-* mice developed normally, and no abnormal physiological features were observed for up to 20 months after their birth. Using capecitabine, we constructed a mouse model of HFS (Fig. S2). After gavage with capecitabine, we evaluated the HFS grade and body weight of mice (Fig. S4C). *TP-/-* mice showed fewer dry lines, scaling and erythema than wild-type mice (Fig. 2b and Fig. S4A). The HFS grade in the *TP-/-* group was significantly lower than that in the wild-type group (Fig. 2c and Fig. S4D). This evidence strongly suggests that TP knockout may impair the efficiency of 5-DFUR conversion into 5-FU in the palmar and plantar areas of the paw, thus decreasing the accumulation of 5-FU in the target tissue and relieving HFS.

Pain is the predominant symptom of hand-foot syndrome. Consequently, a hot-plate test was conducted to assess hind paw thermal hyperalgesia. The paw withdrawal latency of the hind paw in CAP-wt mice was significantly decreased compared to that in control mice (Fig. 2d). No significant difference was observed between the *TP-/-* group and the control animals at any time during the behavioural measurement. Administration of capecitabine produced significant thermal hyperalgesia in the wild-type mice, which was alleviated in the *TP-/-* mice.

Furthermore, H&E staining and quantification of the epidermis and cuticle thicknesses showed that the damage to the epidermis was attenuated in *TP-/-* mice (Fig. 2e, f and Fig. S4B, E). In addition, according to the Ki67 and EdU staining (Fig. 2g, i), *TP-/-* restored the proliferation activity of epidermal basal-layer cells. Capecitabine induced massive immune cell infiltration into the epidermis and dermis of wild-type mice, and these effects were reduced in *TP-/-* mice (Fig. 2h, i). These results clearly show that the expression of TP was elevated in the palm and planta of the paw and provide direct evidence for the involvement of TP in capecitabine-induced HFS. Thus, we conclude that elevated expression of TP in the palm and sole of the paw plays an important role in capecitabine-induced HFS.

Clinical pharmacokinetic studies showed that the plasma AUC of 5-FU reached only 0.46 to 0.69 mg·h/L, more than 20 times lower than that of its direct precursor 5-DFUR (11.7 to 16.0 mg·h/L) (Fig. 1b and Fig. S1A) [20]. Additionally, similar pharmacokinetic profiles were observed in mice (Fig. 1c and Fig. S1B) [38]. Therefore, we used 5-DFUR in vitro to elucidate the intracellular mechanism of keratinocyte cytotoxicity. HaCaT and primary keratinocyte (NHEK) cells were used to explore the toxicity mechanism. HaCaT and NHEK cells were exposed to different concentrations of 5-DFUR for 48 h. 5-DFUR decreased cell proliferation in a dose-dependent manner, as indicated by EdU incorporation and cell counting kit-8 assay (Fig. 3a and Fig. S5A). The phase-contrast images showed that the dying cells exhibited characteristic large bubbles extruding from the plasma membrane, and the cells had typical swelling (Fig. 3b and Fig. S5C), the key characteristics of pyroptosis. Of note, the release of lactate dehydrogenase (LDH) was significantly elevated from HaCaT with an increase in 5-DFUR dosage (Fig. 3c). The release of LDH indicated that treatment with 5-DFUR interrupted the cell membrane integrity. TUNEL staining and flow cytometry analyses of Annexin V and 7-AAD staining assays were performed to further validate the nature of the cell death. As shown in Fig. 3e, the percentage of TUNEL-positive-cells were considerably increased after treatment with 5-DFUR. Compared with mock-treated cells, the percentage of Annexin V and 7-AAD double-positive cells was dramatically increased after 5-DFUR treatment (Fig. 3g, h and Fig. S5E). A similar pattern of pyroptosis was observed in 5-FU-treated keratinocytes as well (Fig. S5A, H, I, J). Combining these findings, we conclude that the metabolites of capecitabine triggered pyroptosis in HaCaT and NHEK cells.

Prior studies have reported that GSDME-mediated proptosis is correlated with the side effects of chemotherapy [30]. Thus, we hypothesized that GSDME might be a key determinant of the effect of 5-DFUR on keratinocytes. To validate this hypothesis, we examined the protein level of the N-terminal domain of cleaved GSDME and found that GSDME cleavage was induced by 5-DFUR in a dose-dependent manner (Fig. 3f and Fig. S5B, D, F). To test whether cleaved caspase-1, -3 or -7 contributed to the cleavage of GSDME, we tested the activation of caspase-1, -3 and -7, which were not detected by western blot (Fig. 3f).

Zhibin et al. reported that killer-cell granzyme B (GrB) could activate caspase-independent pyroptosis in tumour cells by directly cleaving GSDME [39]. Previous studies have reported that keratinocytes can produce granzyme (GrB) under some stress conditions [40, 41]. To determine whether GrB cleaves GSDME, we evaluated the expression of GrB during treatment. As shown by GrB immunofluorescence staining (Fig. 3d), GrB accumulated in cytoplasmic vesicles after 5-DFUR treatment. Furthermore, the mRNA and protein expression levels of GrB were increased (Fig. 3f, i), suggesting that GrB cleaves GSDME. Cleavage of GSDME caused pyroptosis, which in turn increased the secretion of inflammatory factors (Fig. 3i, j and Fig. S5G). Collectively, 5-DFUR induced the production of GrB and the cleavage of GSDME, which punched holes in the cell membrane, causing cell swelling and rupture, releasing inflammatory factors and ultimately resulting in the inflammatory reactions of HFS.

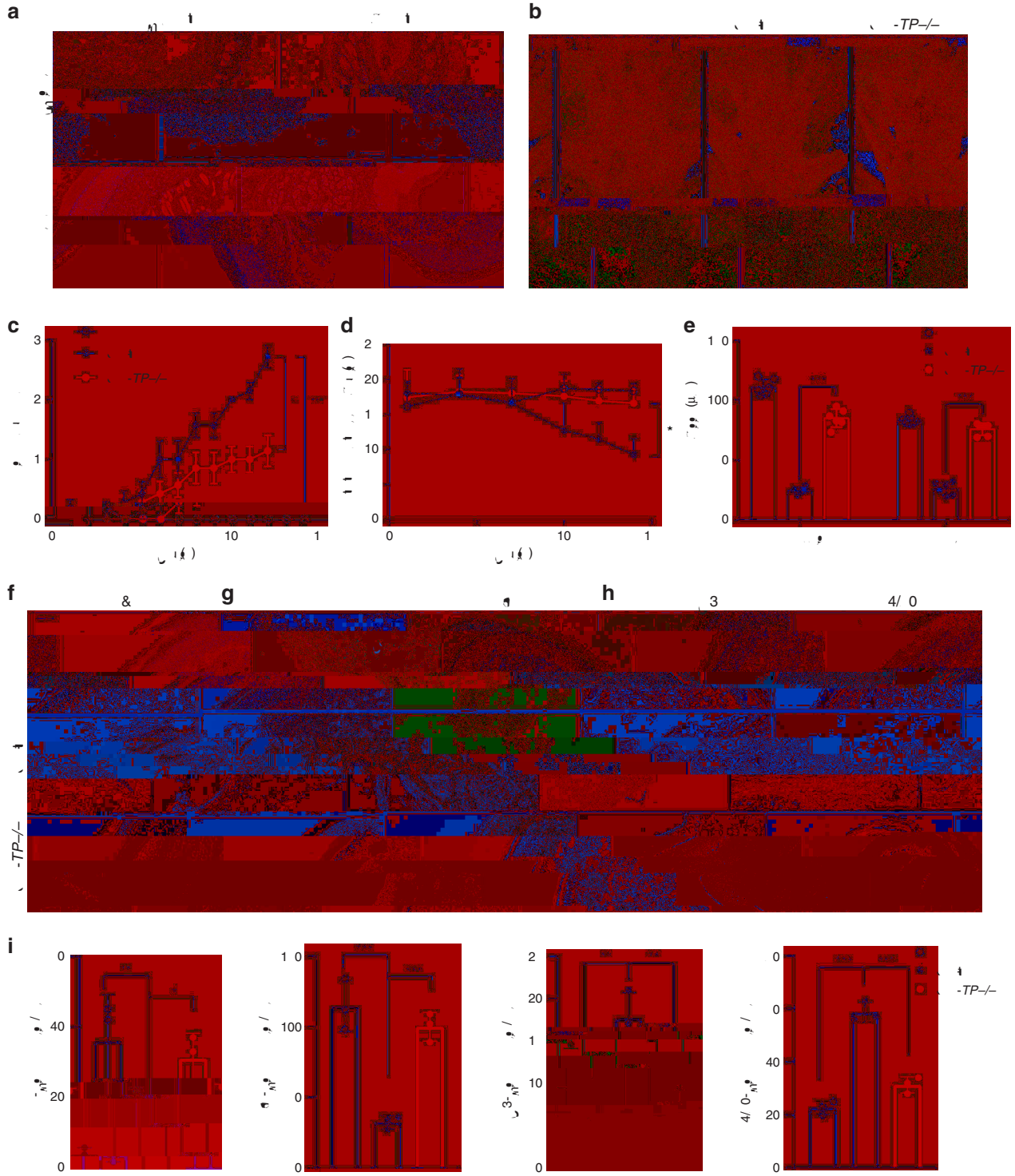

Fig. 2 Thymidine phosphorylase immunoreactivity in the skin of the palm, planta and dorsal paw of wild-type (wt) mice. Representative image of the hind paw of *TP*-/- and wt mice treated with capecitabine (CAP). Mean HFS grade of *TP*-/- and wt mice ($n = 6$). The development of thermal hyperalgesia in the hind paws of *TP*-/- and wt mice treated with CAP ($n = 6$). Quantitative analysis of epidermal damage assessed by measuring the stratum corneum and epidermal thickness ($n = 6$). Representative H&E staining images of mouse hind paws. EdU immunofluorescence staining and Ki67 immunohistochemical staining images of hind paws of *TP*-/- and wt mice treated with CAP. EdU: red; DAPI: blue. Representative CD3 and F4/80 immunohistochemical staining images of mouse hind paws. Morphometric analysis of mice skin tissues. Shown are EdU, Ki67, CD3 and F4/80-positive cells per 200× fields. Ten different microscopic fields per tissue section per animal ($n = 3$/group) were analysed. Scale bar: 100 μm. The results in , , and are presented as the mean ± SEM and mean ± SD. *$P < 0.05$; **$P < 0.01$; ***$P < 0.001$; ns, no significant difference.

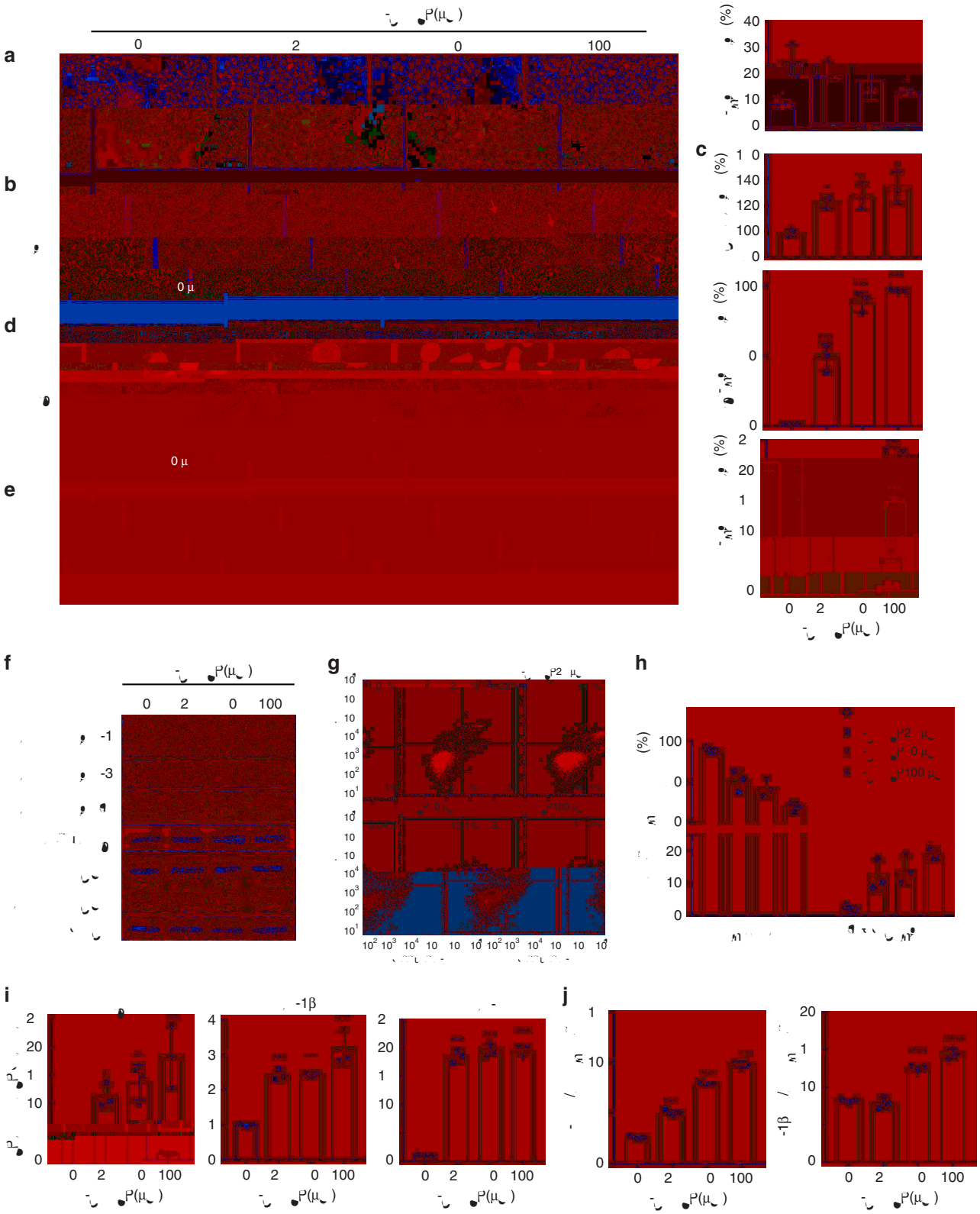

Fig. 3 . Representative images and quantitative data of EdU proliferative live-staining for HaCaT cells in the CTL and 5-DFUR groups after 48 h of treatment ($n = 3$). Representative images of HaCaT cell morphology. Arrows indicate pyroptotic cells. Quantification of LDH release-based cell death in HaCaT cells ($n = 3$). Representative images of GrB immunofluorescence staining and the results of GrB-positive cell analysis ($n = 3$). Representative images of TUNEL staining and the results of TUNEL-positive cells per field ($n = 3$). Western blot of 5-DFUR-induced GSDME cleavage by GrB. Flow cytometry of 7-AAD- and Annexin V-fluorescein isothiocyanate (FITC)-stained cells. Percentage of 7-AAD-positive HaCaT cells treated with 5-DFUR ($n = 3$). 5-DFUR increased the 7-AAD-positive cells in a dose-dependent manner. Relative expression of GrB, IL-1β and IL-6 in HaCaT cells ($n = 3$). IL-1β and IL-6 concentrations in cell culture supernatant measured by ELISA ($n = 3$). Scale bar: 100 μm. The results in , , , , and are presented as the mean ± SD. *$P < 0.05$; **$P < 0.01$; ***$P < 0.001$; ns, no significant difference.

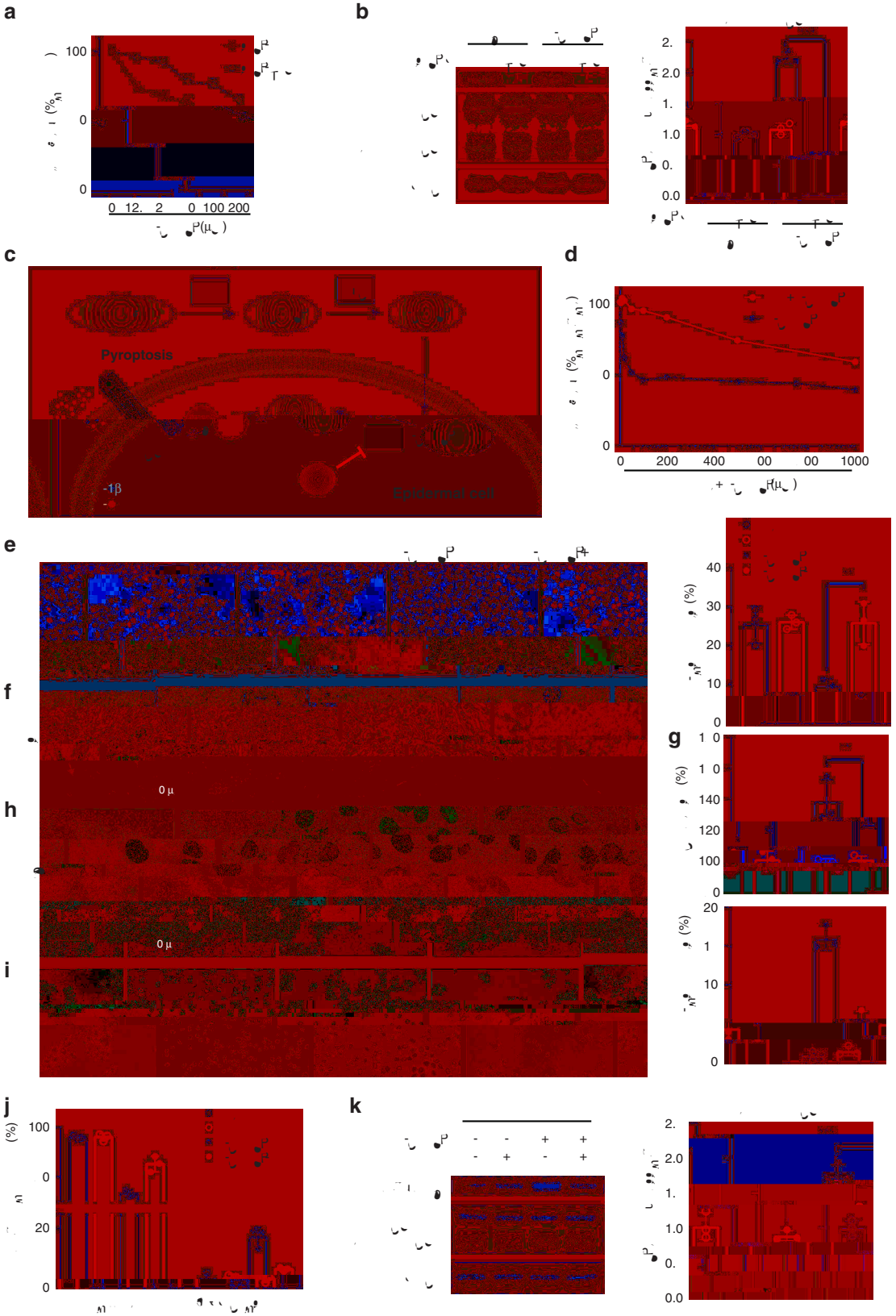

The elevated expression of TP in the palm and sole of the paw plays an important role in capecitabine-induced HFS. The involvement of TP in vitro in regulating the toxicity of 5-DFUR is needed to explore. Thus, we generated *TYMP*-silenced HaCaT cells to examine the influence of TP on 5-DFUR-induced toxicity (Fig. 4b). As a result, silencing *TYMP* significantly increased the

Fig. 4 5- . The cell survival rates of HaCaT cells transfected with non-targeting siRNA or siRNA-targeting *TYMP* after exposure to various concentrations of 5-DFUR. The cleavage of GSDME of HaCaT cells transfected with non-targeting siRNA or siRNA-targeting *TYMP* after exposure to 5-DFUR (50 μM). Relative expression levels of cleaved GSDME compared with GAPDH in HaCaT cells ($n = 3$). Mechanism of protective effects against capecitabine-induced toxicity by TPI. Effect of concurrent treatment with TPI (5 μM) on survival after exposure to various concentrations of 5-DFUR in HaCaT cells. Representative images and quantitative data of EdU proliferative live-staining for HaCaT cells in different treatment groups ($n = 3$). Representative images of HaCaT cell morphology in different treatment groups. Arrows indicate pyroptotic cells. Quantification of LDH release-based cell death of HaCaT cells ($n = 3$). Representative images of GrB immunofluorescence staining. Representative images of TUNEL staining and the results of TUNEL-positive cells per field ($n = 3$). Percentage of 7-AAD-positive HaCaT cells ($n = 3$). Effects of TPI on 5-DFUR-induced GSDME cleavage by GrB. Relative expression levels of cleaved GSDME compared with GAPDH in HaCaT cells ($n = 3$). Scale bar: 100 μm. The results in , , , , , and are presented as the mean ± SD. *$P < 0.05$; **$P < 0.01$; ***$P < 0.001$; ns, no significant difference.

proliferation rate of HaCaT cells after treatment with 5-DFUR (Fig. 4a). The elevated level of cleaved GSDME by 5-DFUR was reversed by silencing *TYMP* (Fig. 4b). Through phase-contrast images, silencing *TYMP* provided a protective effect against 5-DFUR-induced pyroptosis (Fig. S6I). These results suggest that TP involves in 5-DFUR-mediated cell toxicity.

Based on the above results, we proposed that pharmacological inhibition of TP activity to reduce the production of 5-FU and inhibit the development of pyroptosis could be potential treatments for HFS (Fig. 4c). Nevertheless, no specific compound that inhibits GSDME-mediated pyroptosis has yet been identified. The potent and specific TP inhibitor tipiracil (TPI), which was approved by the FDA as a part of the combination therapy for metastatic colorectal cancer [42], became our candidate of interest.

We then studied the ability of TPI against 5-DFUR-induced toxicity. We combined TPI with 5-DFUR to treat HaCaT and NHEK cells for 48 h to demonstrate its ability to alleviate the toxicity of 5-DFUR. As shown in Fig. 4d, e, and Fig. S6G, TPI significantly increased the IC50 of 5-DFUR and the proliferation ability of HaCaT and NHEK cells, as shown by the cell counting kit-8 assay and the EdU staining assay. The phase-contrast images showed that TPI provided a protective effect against 5-DFUR-induced pyroptosis (Fig. 4f and Fig. S6K). Meanwhile, the elevated release of LDH, the percentage of TUNEL-positive cells and the increased percentage of Annexin V and 7-AAD double-positive cells were almost completely reversed by TPI treatment (Fig. 4g, i, j and Fig. S6A, L). The production of GrB and cleavage of GSDME were restored (Fig. 4h, k and Fig. S6H), confirming that TPI relieves pyroptosis. As shown by GrB immunofluorescence staining (Fig. 4h and Fig. S6B), the GrB accumulation in cytoplasmic vesicles induced by 5-DFUR was significantly decreased by TPI. Furthermore, TPI administration markedly reduced the levels of the inflammatory factors IL-1β, IL-6 and IL-18 that were enhanced by 5-DFUR (Fig. S6C, D, E). Based on these results, we believe that TPI could be a potential treatment of capecitabine-induced HFS.

Given the observations that TPI could relieve the pyroptosis induced by 5-DFUR in vitro, we next conducted prevention experiments to evaluated the HFS grade and body weight of mice by topically applying TPI to our HFS mice models (Fig. 5a and Fig. S7B). We topically applied TPI gel or its vehicle gel to the forepaws and hind paws of mice at the beginning of the treatment with capecitabine. TPI showed excellent protective effects as a prophylactic treatment. The HFS grade in the CAP-TPI group was significantly lower than that in the CAP-vehicle group (Fig. 5b, c and Fig. S7A, C). Paw withdrawal latency of the hind paw showed that topical application of TPI gel significantly decreased thermal hyperalgesia produced by capecitabine (Fig. 5d). H&E staining and examination of the epidermis and cuticle thickness showed that the damage to the epidermis was relieved by TPI gel application (Fig. 5e, f and Fig. S7D, E). In addition, according to the Ki67 and EdU staining (Fig. 5g, i), TPI restored the proliferative activity of epidermal basal-layer cells. Immunohistochemistry analyses showed that the topical application of TPI decreased the infiltration of lymphocytes and macrophages (Fig. 5h, i and Fig. S7D), which showed that TPI relieved inflammatory responses in capecitabine-induced HFS. Hence, we concluded that topical application of TPI could be an effective intervention strategy against capecitabine-induced HFS.

Topical treatment with TPI could possibly reduce the incidence and severity of HFS during anticancer therapy. Therefore, it is important to establish that the anticancer efficacy of capecitabine is not reduced by TPI. To this end, we evaluated the tumour growth in the HCT116 xenograft murine tumour model receiving oral administration of capecitabine and topical application of TPI gel or the vehicle gel. Body weight, which also reflected the tumour growth, was monitored during the experiment (Fig. 6a) and showed no significant fluctuation among the three groups. We observed reduced tumour growth and tumour volume in the groups treated with capecitabine (180 mg/kg) and topical application of TPI gel or vehicle gel compared with the control group (Fig. 6b, c). The time course of the responses revealed that capecitabine significantly inhibited the tumour growth of the CAP-vehicle group ($534.7 \pm 71.32\ mm^3$) and CAP-TPI group ($496.4 \pm 30.67\ mm^3$) compared to control mice ($1557 \pm 456\ mm^3$). Tumours from each group were collected and weighed at the end of this experiment. The decrease in tumour weight was significantly greater in the capecitabine-treated mice CAP-vehicle group ($0.374 \pm 0.0.095$ g) and CAP-TPI group (0.316 ± 0.125 g) than in the control mice (3.026 ± 0.538 g). There was no significant difference in body weight, tumour volume or tumour weight between the CAP-TPI and CAP-vehicle groups (Fig. 6a, b, d). These results suggested that topical TPI did not affect the antitumor effect of capecitabine and that TPI was well tolerated in the human colorectal cancer xenograft model.

HFS is a common dose-limiting toxicity of capecitabine, occurring in up to 71% of patients [9]. HFS can progress to an extremely painful and debilitating condition, causing significant discomfort and impairment of function, potentially leading to worsened quality of life in patients receiving capecitabine [43]. It is essential to understand the pharmacological basis of HFS to provide a rationale for preventive or curative interventions.

Our findings suggest that the mechanism for capecitabine-induced HFS is related to the activity of TP, which is responsible for the metabolism of 5-DFUR into 5-FU. The concentrations and distributions of 5-DFUR and 5-FU supported the hypothesis that capecitabine-induced HFS is dependent on the activity of TP. An elevated expression of TP may cause high localised concentrations of 5-FU and lead to epidermal toxicity [25]. In our study, TP expression was significantly higher in the palmar and plantar areas than in the dorsal area of the paw, which is consistent with the results of a previous study.

To further explore the theory that overexpression of TP in the target tissue induces the development of HFS, we generated *TP-/-*

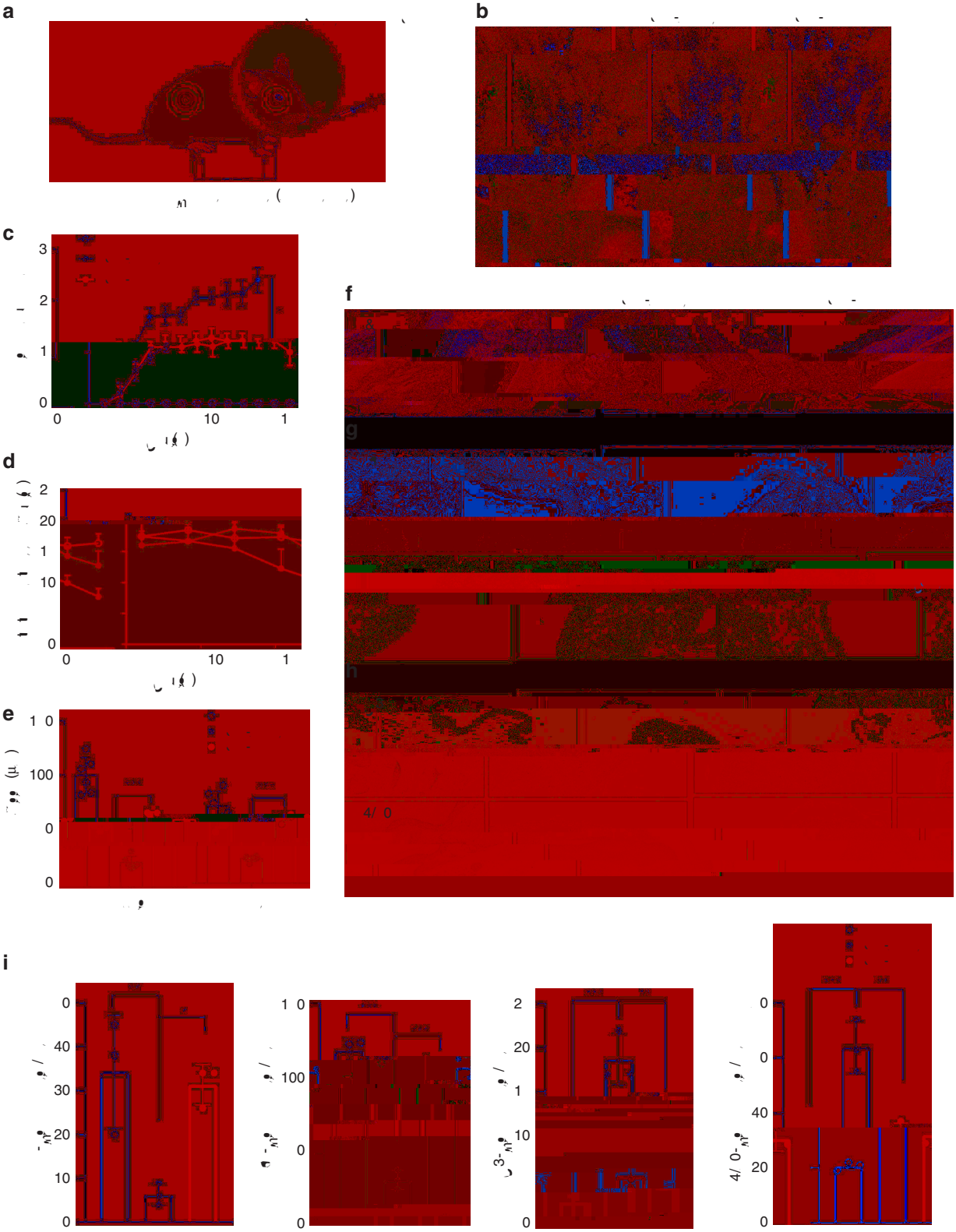

mice, which appeared physically and behaviourally normal compared with wild-type mice. *TP-/-* mice were quite resistant to the HFS induced by capecitabine. Capecitabine disrupted the proliferation of the basal-layer cells, induced scaling and redness, and caused immune cell infiltration into the paws of wild-type mice, and these effects were attenuated in *TP-/-* mice. These results provide direct evidence that TP is involved in the development of HFS. Thus, we concluded that the expression of TP plays an important role in capecitabine-induced HFS.

For the first time, our study revealed that capecitabine and its metabolites kill epidermal cells through GSDME-mediated pyroptosis. Earlier studies demonstrated that apoptosis is the primary

Fig. 5 . Schematic of the mouse experimental methodology. CAP: capecitabine 1000 mg/kg; TPI gel: 2% tipiracil gel. Representative images of the hind paws of mice treated with oral CAP and topical application of TPI or vehicle gel. Mean HFS grade of mice treated with TPI or vehicle gel ($n = 6$). The development of thermal hyperalgesia in the hind paws of mice treated with oral CAP and topical application of TPI or vehicle gel ($n = 6$). Quantitative analysis of epidermal damage assessed by measuring the stratum corneum and epidermal thickness ($n = 6$). Representative H&E staining and Ki67, CD3 and F4/80 immunohistochemical staining and EdU immunofluorescence staining of the hind paws of the mice. Morphometric analysis of mice skin tissues. Shown are EdU, Ki67, CD3 and F4/80-positive cells per 200× fields. Ten different microscopic fields per tissue section per animal ($n = 3$/group) were analysed. Scale bar: 100 μm. The results in , and are presented as the mean ± SEM and mean ± SD. *$P < 0.05$; **$P < 0.01$; ***$P < 0.001$; ns, no significant difference.

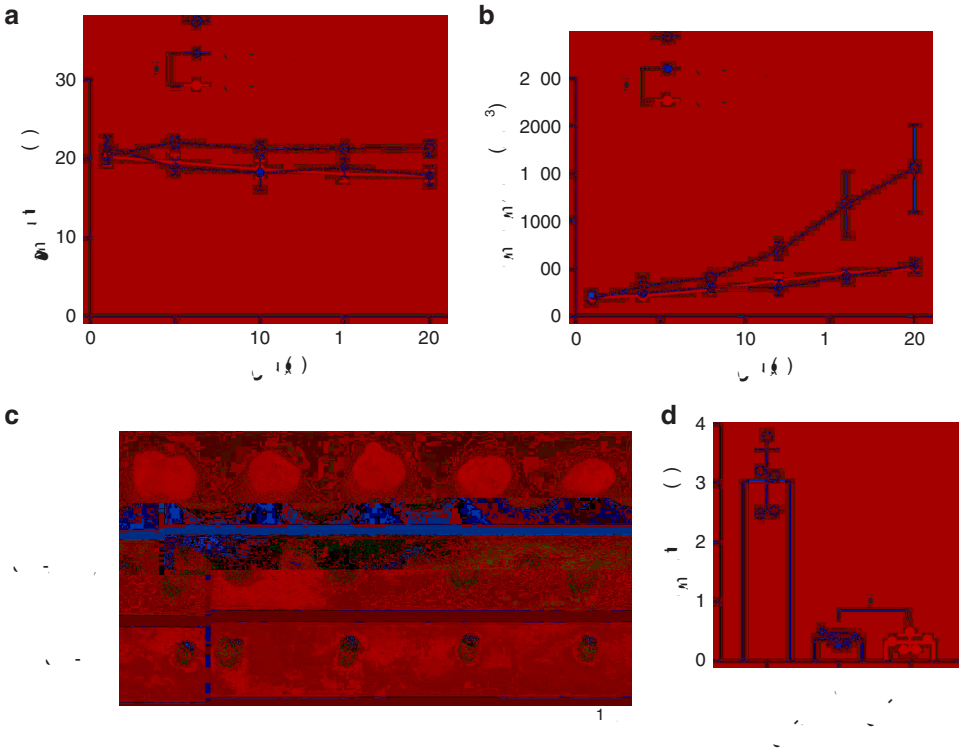

Fig. 6 . CTL: mice gavaged with solvent. CAP-Vehicle: mice gavaged with capecitabine (180 mg/kg) and topically treated with vehicle gel. CAP-TPI: mice gavaged with capecitabine (180 mg/kg) and topically treated with 2% TPI gel. , Body weight and tumour volume changes in HCT 116 human colon cancer xenograft mice in different groups ($n = 5$). Representative pictures of xenograft tumours from nude mice. Quantitative analysis of tumour weights at the time of sacrifice ($n = 5$). The results in , and are presented as the mean ± SEM. *$P < 0.05$; **$P < 0.01$; ***$P < 0.001$; ns, no significant difference.

type of cell death associated with fluoropyrimidine [26]. However, we observed characteristic large bubbles emerging from the plasma membrane after exposure of HaCaT and NHEK cells to 5-DFUR and 5-FU, implying the induction of pyroptosis. Moreover, GSDME was activated in a concentration-dependent manner following treatment with 5-DFUR, implying that 5-DFUR-induced pyroptosis of keratinocytes is GSDME dependent. Pyroptosis can be induced by caspase family activation via GSDMD/GSDME cleavage, leading to cell bubbling and the release of IL-1β [44]. In this study, the activation of caspase-1, -3 and -7 was not detected, which may suggest that these proteins were not involved in GSDME-mediated pyroptosis in HaCaT cells. In addition, GrB has been reported to cleave GSDME, similar to caspase-3, and induce pyroptosis [39]. Herein, we found that GrB accumulated after 5-DFUR treatment, indicating that GrB might directly cleave GSDME and activate pyroptosis. Taken together, we have found that the metabolites of capecitabine, both 5-DFUR and 5-FU, induces pyroptosis in human epidermal cells via GrB/GSDME signalling, and then it triggers acute inflammatory reactions, which may advance our understanding of chemotherapy-induced toxicities.

To further investigate the involvement of TP on HFS in vitro, we constructed *TYMP* knockdown HaCaT cells. *TYMP* knockout increased cell proliferation ability, prevented GSDME activation and subsequent pyroptosis in keratinocytes, implying that TP is involved in keratinocytes pyroptosis induced by 5-DFUR.

Our findings imply, in theory, two potential intervention strategies against capecitabine-induced HFS, namely, the topical application of TP inhibitors and the inhibition of pyroptosis. However, compounds that can block pyroptosis are still in preclinical investigation, and the date of their clinical approval is as yet undetermined. In contrast, tipiracil (TPI), a selective TP inhibitor, has been approved by the Food and Drug Administration for clinical use [42]. Its effectiveness against 5-DFUR-induced cytotoxicity was well demonstrated in HaCaT and NHEK cells, followed by favourable outcomes in treating capecitabine-induced HFS in our mouse models. In addition, we tested the influence of TPI on cancer therapy in vivo. The results showed that topical use of TPI did not affect the antitumor efficacy of capecitabine. Based on these positive results, we believe TPI can be a promising therapeutic drug for treating capecitabine-induced HFS.

In summary, our research reveals that the elevated expression of TP in the palmar and plantar skin is a critical factor in capecitabine-induced HFS, wherein *TP-/-* mice were effectively protected from cutaneous toxicity. We further identified GSDME-mediated pyroptosis as the precise mechanism underlying this toxicity system. More importantly, based on the mechanistic findings, TPI was identified as a highly effective drug against capecitabine-induced HFS. These findings not only shed light on the aetiology of capecitabine-induced HFS but also provide a promising intervention strategy using TP inhibitors to mitigate the debilitating side effects associated with capecitabine.

A A A A A

All data associated with this study are present in the paper or the Supplementary Materials.

. . .

1. Walko CM, Lindley C. Capecitabine: a review. Clin Ther. 2005;27:23–44.
2. Oevermann K, Buer J, Hoffmann R, Franzke A, Schrader A, Patzelt T, et al. Capecitabine in the treatment of metastatic renal cell carcinoma. Br J Cancer. 2000;83:583–7.
3. Kang HJ, Chang HM, Kim TW, Ryu MH, Sohn HJ, Yook JH, et al. A phase II study of paclitaxel and capecitabine as a first-line combination chemotherapy for advanced gastric cancer. Br J Cancer. 2008;98:316–22.
4. Saif MW, Katirtzoglou NA, Syrigos KN. Capecitabine: an overview of the side effects and their management. Anticancer Drugs. 2008;19:447–64.
5. Nagore E, Insa A, Sanmartín O. Antineoplastic therapy—induced palmar plantar erythrodysesthesia ('hand-foot') syndrome. Am J Clin Dermatol. 2000;1:225–34.
6. Saif MW. Capecitabine and hand–foot syndrome. Expert Opin Drug Saf. 2011;10:159–69.
7. Zielinski C, Lang I, Beslija S, Kahan Z, Inbar MJ, Stemmer SM, et al. Predictive role of hand–foot syndrome in patients receiving first-line capecitabine plus bevacizumab for HER2-negative metastatic breast cancer. Br J Cancer. 2016;114:163–70.
8. Van Cutsem E, Twelves C, Cassidy J, Allman D, Bajetta E, Boyer M, et al. Oral capecitabine compared with intravenous fluorouracil plus leucovorin in patients with metastatic colorectal cancer: results of a large phase III study. J Clin Oncol. 2001;19:4097–106.
9. Fumoleau P, Largillier R, Clippe C, Dièras V, Orfeuvre H, Lesimple T, et al. Multicentre, phase II study evaluating capecitabine monotherapy in patients with anthracycline- and taxane-pretreated metastatic breast cancer. Eur J Cancer. 2004;40:536–42.
10. Lassere Y, Hoff P. Management of hand-foot syndrome in patients treated with capecitabine (Xeloda®). Eur J Oncol Nurs. 2004;8:S31–40.
11. Baack BR, Burgdorf WHC. Chemotherapy-induced acral erythema. J Am Acad Dermatol. 1991;24:457–61.
12. Fitzpatrick JE. The cutaneous histopathology of chemotherapeutic reactions. J Cutan Pathol. 1993;20:1–14.
13. Degen A, Alter M, Schenck F, Satzger I, Völker B, Kapp A, et al. The hand-foot-syndrome associated with medical tumor therapy–classification and management. JDDG: J der Dtsch Dermatologischen Ges. 2010;8:652–61.
14. Narasimhan P, Narasimhan S, Hitti IF, Rachita M. Serious hand-and-foot syndrome in black patients treated with capecitabine: report of 3 cases and review of the literature. Cutis. 2004;73:101–6.
15. van Doorn L, Veelenturf S, Binkhorst L, Bins S, Mathijssen R. Capecitabine and the Risk of Fingerprint Loss. JAMA Oncol. 2017;3:122–3.
16. Gressett SM, Stanford BL, Hardwicke F. Management of hand-foot syndrome induced by capecitabine. J Oncol Pharm Pract. 2006;12:131–41.
17. Lassere Y, Hoff P. Management of hand-foot syndrome in patients treated with capecitabine (Xeloda). Eur J Oncol Nurs. 2004;8:S31–40.
18. Miwa M, Ura M, Nishida M, Sawada N, Ishikawa T, Mori K, et al. Design of a novel oral fluoropyrimidine carbamate, capecitabine, which generates 5-fluorouracil selectively in tumours by enzymes concentrated in human liver and cancer tissue. Eur J Cancer. 1998;34:1274–81.
19. Diasio RB, Harris BE. Clinical pharmacology of 5-fluorouracil. Clin Pharmacokinet. 1989;16:215–37.
20. Reigner B, Blesch K, Weidekamm E. Clinical pharmacokinetics of capecitabine. Clin Pharmacokinet. 2001;40:85–104.
21. Saif MW, Juneja V, Black G, Thronton J, Johnson MR, Diasio RB. Palmar-plantar erythrodysesthesia in patients receiving capecitabine and intratumor thymidine phosphorylase and dihydropyrimidine dehydrogenase: is there a pharmacologic explanation? Support Cancer Ther. 2007;4:211–8.
22. Asgari MM, Haggerty JG, McNiff JM, Milstone LM, Schwartz PM. Expression and localization of thymidine phosphorylase/platelet-derived endothelial cell growth factor in skin and cutaneous tumors. J Cutan Pathol. 1999;26:287–94.
23. Merk, HF. Drug skin metabolites and allergic drug reactions. Curr Opin Allergy Clin Immunol. 2009;9:311–5.
24. Sharma AM, Uetrecht J. Bioactivation of drugs in the skin: relationship to cutaneous adverse drug reactions. Drug Metab Rev. 2014;46:1–18.
25. Milano G, Etienne-Grimaldi M-C, Mari M, Lassalle S, Formento J-L, Francoual M, et al. Candidate mechanisms for capecitabine-related hand-foot syndrome. Br J Clin Pharmacol. 2008;66:88–95.
26. Ricci, MS, Zong, W-X. Chemotherapeutic approaches for targeting cell death pathways. Oncologist. 2006;11:342–57.
27. Tan Y, Chen Q, Li X, Zeng Z, Xiong W, Li G, et al. Pyroptosis: a new paradigm of cell death for fighting against cancer. J Exp Clin Cancer Res. 2021;40:153.

all experiments. SZ reviewed and edited the manuscript. All authors approved the paper.

This work was supported by the Youth Thousand Talents Programme of China, start-up grants from the Shanghai Jiao Tong University (WF220408211). This work was also supported by the grants from the State Key Laboratory of Onco- genes and Related Genes (90-17-02) and from the Interdisciplinary Programme of Shanghai Jiao Tong University (YG2017MS18).

The authors declare no competing interests.

Not applicable.

The online version contains supplementary material available at https://doi.org/10.1038/s41416-022-02039-3.

and requests for materials should be addressed to Shiyi Zhang.

is available at http://www.nature.com/reprints

Springer Nature remains neutral with regard to jurisdictional claims in published maps and institutional affiliations.